Anisotropic poroelasticity – Does it apply to shale?

Rune M Holt, NTNU; Audun Bakk, SINTEF and Andreas Bauer, SINTEF and NTNU

Summary

Shale plays an important role as cap rock above oil and gas reservoirs and above e.g. CO_2 storage sites, as well as being source and reservoir rock in development of so-called unconventional reserves. Shale anisotropy needs to be accounted for in geophysical as well as geomechanical applications. This paper presents a brief description of anisotropic poroelasticity theory, and compares it to its more familiar isotropic counterpart. Experiments performed with field shales are presented, and the static mechanical behavior in terms of drained versus undrained moduli, Skempton parameters and Biot coefficients are shown to be consistent with the poroelastic approach. The necessary steps to provide static properties from seismic data and further link these measurements to laboratory ultrasonic data are briefly discussed.

Introduction

Poroelasticity theory is well established in 4D seismic analysis of fluid substitution in conventional reservoir rocks. In shales, however, poroelastic applications are less frequent. One reason is that shale has very low permeability (in the nanoDarcy range) and that mechanical properties of shale are fluid sensitive. Hence, some of the basic requirements for classical poroelasticity theory to be valid may be violated. Further, shales are anisotropic: Obviously, the need to deal with five different stiffnesses and three additional poroelastic parameters even in the simplest case of TI (transverse isotropy) symmetry (Cheng, 1997) makes field applications challenging. However, application of an isotropic poroelastic model may lead to significant errors. An example is the undrained pore pressure response (Holt et al., 2017), which depends on Skempton's parameters (Skempton, 1954). Skempton's A = 1/3 in isotropic poroelasticity. However, in a TI poroelastic medium A becomes a natural part of a 2nd rank Skempton tensor. Experiments confirm that A depends on orientation of the stress field with respect to the symmetry axis, and that A may be very different from 1/3, as predicted by anisotropic poroelasticity. This may have profound impact on predicted pore pressure changes in rocks surrounding a depleting or inflating reservoir, affecting infill drilling and the risk of induced seismicity. Another example is evaluation of static geomechanical properties of overburden shale or of shale reservoirs from seismic (or sonic logging). Since static and dynamic properties of rocks in general are different, the transforming procedure needs to account for anisotropy.

Here we first present first key ingredients of anisotropic poroelasticity in comparison with the more familiar isotropic approach. Laboratory experiments with shale cores are then analyzed to see to what extent static data are consistent with current anisotropic poroelasticity theory. Finally, we will discuss how such an analysis can be extended to link static mechanical properties to their seismic and ultrasonic counterparts.

Anisotropic poroelasticity

Poroelasticity theory is based on pioneering work by e.g. Gassmann (1951) and Biot (1962). The isotropic approach is described in several textbooks, such as Fjær et al. (2008). The basic assumptions behind these theories are homogeneous, linearly elastic, porous and permeable media. The key result is the tie between drained (subscript dr) and undrained (subscript u) moduli, expressed by the Biot-Gassmann equation for the bulk modulus K:

$$K_{\mathrm{u}} = K_{\mathrm{dr}} + \alpha^2 M\,, \tag{1}$$

where the Biot coefficient

$$\alpha = 1 - \frac{K_{\mathrm{dr}}}{K_{\mathrm{s}}}\,, \tag{2}$$

and the M-parameter is given by:

$$\frac{1}{M} = \frac{\alpha - \phi}{K_{\mathrm{s}}} + \frac{\phi}{K_{\mathrm{f}}}\,. \tag{3}$$

Here K_{f} is the pore fluid bulk modulus, K_{s} is the solid grain bulk modulus, and ϕ is the porosity. The drained rock is assumed insensitive to pore fluid, hence K_{dr} is a fluid-independent constant, and the undrained and drained shear moduli (G) are equal:

$$G_{\mathrm{u}} = G_{\mathrm{dr}} \tag{4}$$

The pore pressure (p_{f}) evolution in an undrained hydrostatic experiment defines Skempton's B parameter (Skempton, 1954), given by (σ is the external stress):

$$\frac{\Delta p_{\mathrm{f}}}{\Delta \sigma} = B = \frac{\alpha M}{K_{\mathrm{u}}}\,, \tag{5}$$

Using the Voigt notation, the TI version of the Biot-Gassmann equation (Eq. (3)), can be written (Collet and Gurevich, 2013)

$$C_{\mathrm{ij,u}} = C_{\mathrm{ij,dr}} + \alpha_{\mathrm{i}}\alpha_{\mathrm{j}} M\,. \tag{6}$$

There are now two Biot coefficients (α_{V} and α_{H}, where indices V and H refer to vertical (symmetry axis, associated with subscript 3) and horizontal (symmetry plane, subscripts 1 and 2), respectively):

$$\alpha_{\mathrm{H}} = 1 - \frac{C_{11,\mathrm{dr}} + C_{12,\mathrm{dr}} + C_{13,\mathrm{dr}}}{3K_{\mathrm{s}}} \tag{7}$$

$$\alpha_{\mathrm{V}} = 1 - \frac{C_{33,\mathrm{dr}} + 2C_{13,\mathrm{dr}}}{3K_{\mathrm{s}}}$$

Notice that $C_{12}=C_{11}-2C_{66}$, and that C_{66}, being a shear modulus, is assumed equal in drained and undrained conditions (cfr. Eq. (4)). M can be expressed in the same way as for the isotropic case (Eq. (3)), with the Biot coefficient replaced by the mean value of the two Biot coefficients above, i.e.

$$\frac{1}{M}=\frac{<\alpha>-\phi}{K_s}+\frac{\phi}{K_f} \quad , \tag{8}$$

with $<\alpha>=\frac{\alpha_V+2\alpha_H}{3}$. Notice that the mean value of α also can be written

$$<\alpha>=1-\frac{K_{dr}^0}{K_s}, \tag{9}$$

where K_{dr}^0 is the drained bulk modulus obtained under isotropic strain conditions:

$$K_{dr}^0=K_{dr}=\frac{2(C_{11,dr}+C_{12,dr})+C_{33,dr}+4C_{13,dr}}{9}. \tag{10}$$

In these equations, K_s is assumed to be isotropic. This is clearly not correct, since clay minerals are known to be strongly anisotropic (Sayers and den Boer, 2016). Also, the solid frame consists of different solid minerals, whereas the model treats the solid as homogeneous. Still, to preserve simplicity, at least as a starting point, this assumption is kept in our analysis below. A more thorough analysis should incorporate the formulation by Brown and Korringa (1975) and elaborated further by Thomsen (2017).

The TI poroelastic material has two different Skempton parameters, defined by a 2nd rank Skempton tensor (B_{ij}):

$$\frac{\Delta p_f}{\Delta\sigma_{ij}}=\frac{1}{3}B_{ij}. \tag{11}$$

As for any 2nd rank tensor in TI symmetry, the Skempton tensor has two principal components that can be denoted B_H and B_V. These are invariant with respect to rotation of the coordinate system. The traditional Skempton parameters relate to the invariants as

$$B=\frac{2B_H+B_V}{3} \tag{12}$$

and

$$A=\frac{(B_H\sin^2\theta+B_V\cos^2\theta)}{3B}. \tag{13}$$

Notice that A depends on the angle θ between the symmetry axis and the direction of the maximum principal stress. The Biot coefficients relate to the Skempton parameters as follows (Cheng, 1997):

$$\begin{aligned}3M\alpha_H&=(C_{11,u}+C_{12,u})B_H+C_{13,u}B_V\\3M\alpha_V&=2C_{13,u}B_H+C_{33,u}B_V\end{aligned}. \tag{14}$$

This is equivalent to Eq. (5) in isotropic poroelasticity. Considering only Skempton's B, Eq. (14) can be written in the same way as Eq.(5):

$$B=\frac{<\alpha^*>M}{K_u^*}. \tag{15}$$

The asterisk indicates that the drained bulk modulus in $<\alpha^*>$ and in K_u^* is obtained under isotropic stress conditions:

$$K_{dr}^*=\frac{(C_{11,dr}+C_{12,dr})C_{33,dr}-2C_{13,dr}^2}{(C_{11,dr}+C_{12,dr})+2C_{33,dr}-4C_{13,dr}}. \tag{16}$$

Laboratory experiments

Laboratory experiments have been performed on different field shales permitting application and measurement of external axial and confining ("radial") stress plus pore pressure. Axial and radial strains are measured simultaneously with multidirectional ultrasonic P- and S-wave velocities. The tests have been performed at elevated stress and pore pressure, mimicking in situ conditions for each shale core. The shales are contacted by brine having equivalent salinity of the anticipated pore fluid throughout the test.

As an example, Figure 1 shows the timeline of a test with a soft shale having 36 % porosity and 72 % clay content. The z-axis of the sample was parallel to the symmetry axis. After reaching target stress, this sample was first unloaded and reloaded in drained conditions, giving a drained (iso-stress) bulk modulus of ~ 0.8 GPa. The next cycle was done with constant net stress. In principle, this provides solid grain bulk modulus, but the small strains (~ 10^{-4}) makes the estimated solid bulk modulus (~ 40 GPa) particularly uncertain due to possible influence of creep or shale-fluid interactions. Following the drained cycles, four different undrained stress path cycles were applied: Incrementally isotropic, uniaxial strain, uniaxial loading and constant mean stress. In this test, the axial stress change was 5 MPa in all cycles. A similar test (without the drained and the constant net stress cycles) was performed with a stiff shale having 15 % porosity and 57 % clay content. In both cases, all five C_{ij}'s for TI can be determined at ultrasonic frequencies from one core plug only. Determination of all five static moduli requires experiments with three differently oriented core plugs: $C_{33,u}$ and $C_{13,u}$ are determined from the undrained uniaxial strain cycle in the test with the 0° (angle ref. bedding normal) sample (Figure 1), whereas $C_{11,u}$ and $C_{66,u}$ (or $C_{12,u}$) require data from both 0 and 90° samples. $C_{44,u}$ is computed from a test with a 45° sample, but is not considered here, since it does not enter the poroelastic inversion procedure. The two Skempton parameters are determined from the stress path dependent pore pressure response (using only one core

plug). Table 1 shows the measured static properties for these two shales, hereafter termed "Soft" (high porosity) and "Stiff" (lower porosity).

An additional set of experiments was performed with core plugs from the same shales in a different triaxial apparatus, using a low frequency (1 – 150 Hz) set-up, where strain amplitudes are 10^{-6} or smaller (see Szewczyk et al., 2017, for more details). This set-up permits all five C_{IJ}'s to be measured at seismic frequencies, again utilizing three core plugs with different orientations. The low frequency tests were done with in situ effective (net) stresses, applying an initial pore pressure of 2 MPa. Undrained static pore pressure changes were measured during the tests, applying the same stress path cycles as above.

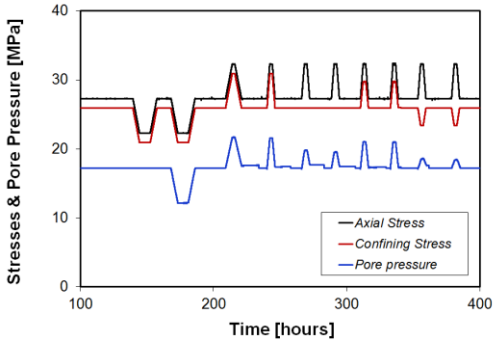

Figure 1: Experimental timeline for the test with the Soft shale (core oriented with axial stress parallel to the symmetry axis). The first two unload-reload cycles were done with controlled pore pressure (drained and constant net stress). The subsequent pairs of load-unload cycles were all undrained, with pore pressure measured, following incrementally isotropic, uniaxial stress, uniaxial strain and constant mean stress paths.

Table 1: Undrained static stiffness parameters and Skempton parameters A and B derived from the tests with a soft and a stiff shale applying different stress paths. Moduli are given in [GPa], Skempton's A is given for a core with sample axis parallel to the symmetry axis ($\theta = 0$).

	C_{11_u}	C_{13_u}	C_{33_u}	C_{66_u}	B	A (0)
Soft	7.60	5.60	7.30	1.30	0.87	0.53
Stifff	24.20	11.20	21.10	7.00	0.72	0.44

Experimental analysis

With knowledge of the undrained moduli and the Skempton parameters from experimental data, one may (following Cheng, 1997) invert Eqs. (6), (7) and (14) for the two Biot coefficients, plus M and K_s. This procedure leads to large uncertainty in prediction of the solid bulk modulus K_s when the value of one or both Biot coefficients is close to 1, typically values one would expect for a soft shale. One alternative is to suggest a reasonable value for K_s. The experimental data do not permit sufficiently accurate estimate of this parameter from constant net stress segments. Use of solid moduli for clay minerals from the literature to calculate e.g. Voigt-Reuss-Hill average based on the mineralogical composition from XRD analysis is feasible. The challenge is however that the literature is wide-spread in terms of clay mineral data: Solid moduli of common constituents such as montmorillonite and kaolinite vary from 5-10 GPa to 40 – 60 GPa (Wang et al., 2001; Mondol et al., 2008; Vanorio et al., 2003). There may be several reasons for this discrepancy, including uncertainty in measurements and extrapolation procedures, clay mineral anisotropy, and the state of the clay minerals inside the shale. Water on surfaces and inside clay minerals may to a varying degree occur as bound water (Holt and Kolstø, 2017), having shear rigidity, and may hence under some conditions act as part of the solid and in other cases as part of the pore fluid. In the present analysis, the value of K_s was constrained by our knowledge of porosity and of the bulk modulus of the pore fluid: K_f is computed from known brine salinity and applied pore pressure, using empirical relations in Batzle and Wang (1992). The computed value of M is the used to estimate K_s by Eq. (8). The resulting calculated parameters are given in Table 2. These parameters further enable calculation of all drained moduli through Eq. (6).

Table 2 Calculated values of the Biot coefficients, the poroelastic modulus M, the solid bulk modulus and the drained iso-stress bulk modulus, using the approach described above. In blue print are the bulk modulus of the pore fluid and the porosity.

	$<\alpha>$	α_V	α_H	M [GPa]	K_s [GPa]	K_{dr} [GPa]	K_f [GPa]	ϕ
Soft	0.91	0.97	0.88	5.8	14.1	1.2	2.71	0.36
Stiff	0.75	0.78	0.73	14.3	27.7	6.9	3.05	0.15

The experiments do not directly provide the Biot coefficients at in situ conditions. However, the axial and radial strains recorded during the different undrained stress path cycles should be consistent with the calculated parameters. Notice, as said above, that some of these strains were used in the inversion procedure. Figure 2 shows calculated axial and radial strains (normalized with respect to axial stress changes; hence they are denoted as compressibilities) for the Soft shale, based on the properties given in Table 2, plus the drained moduli computed with Eq. (6). The agreement between experiment and calculation demonstrates the consistency of the approach, which also implies that anisotropic poroelasticity theory gives an adequate description of the static elastic behavior of this shale. It also implies that sample heterogeneity is small, since data from different cores were utilized. The dashed curves in this figure represent slight improvements by adjusting the Biot coefficients and the M parameters ($\alpha_V \rightarrow 0.99$, $\alpha_H \rightarrow 0.89$, $M \rightarrow 6.1$ GPa). This gives a drained iso-stress bulk modulus of 0.9 GPa, in good agreement with the directly measured value. These adjustments are in line with

predictions of the Brown-Korringa theory as described by Thomsen (2017), but the differences shown are marginal with respect to experimental uncertainty. Figure 3 shows a similar plot for the Stiff shale. Notice that strains are much smaller than in the Soft shale. Here the fit provided by anisotropic poroelasticity can not be improved significantly by adjustments of the Biot coefficients nor *M*, again having experimental uncertainty in mind.

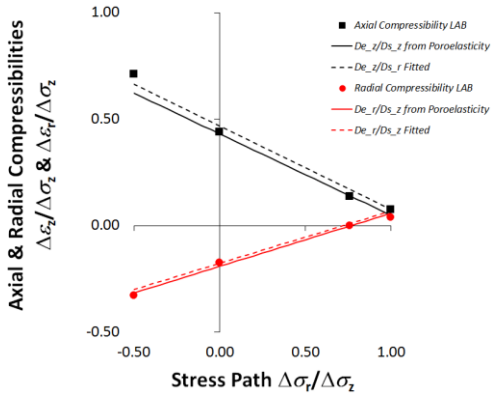

Figure 2 Axial and radial compressibilities versus stress path for the Soft shale. Laboratory data are shown, along with back-calculated strains from the inverted poroelastic parameters in Table 2 (solid lines, see text for further description). The dashed lines are based on an improved fit with slightly modified input parameters (given in text).

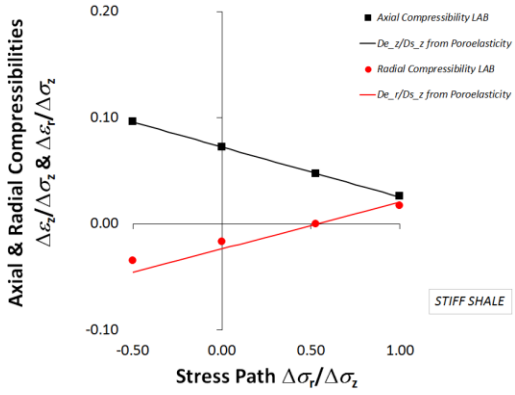

Figure 3 Axial and radial compressibilities versus stress path for the Stiff shale. Laboratory data are shown, along with back-calculated strains from the inverted poroelastic parameters in Table 2 (see text for further description).

Link to seismic and ultrasonic data

Our main reason for addressing the validity of anisotropic poroelasticity theory is to seek a framework where static, seismic and ultrasonic properties can be linked. In the previous section, only static measurements were shown. These are done within finite stress changes and finite strains, and even if the behavior appears linear and non-hysteric, experiments have shown that static moduli only represent truly elastic behavior in the limit of zero stress change (Fjær et al., 2016). Experiments have revealed linearity in compressibility change with stress decrease from an initial state, and if properly calibrated, this may be used as a predictive tool to identify the true elastic moduli. This will, provided there is no dispersion in the sub Hz frequency range, explain the gap between static and seismic moduli. From our experiments we find that the drained P-wave moduli for the Soft shale in the static experiments have to be increased by factors of 3.5 – 4 and the shear moduli by 1.5 – 2.5 to convert the static moduli to those measured at 1 Hz in the seismic experiments. The corresponding conversion factors are considerably smaller for the Stiff shale.

Ultrasonic to seismic conversion involves only dispersion, since both measurements are done in the zero-strain limit. Significant dispersion in shale is observed between seismic (Hz) and ultrasonic (MHz) frequencies (Szewczyk et al., 2017). Complete physical understanding of dispersion in shale is still lacking. A local flow model is likely to apply, but the behavior of bound water may also contribute. Nevertheless, simply reducing porosity to account for the soft pores that are stiffened in the ultrasonic frequency range provides a simple but incomplete way of translating between seismic and ultrasonic moduli.

Conclusions

Experiments with field shale cores verify that anisotropic poroelasticity theory based on Gassmann's equations adequately describe static behavior in terms of undrained vs drained moduli, Skempton parameters and Biot coefficients. This forms a basis for using and extending such theory to link seismic and static behavior through proper description of non-elastic effects on drained moduli. Static and seismic properties can be linked to ultrasonic moduli within the same framework by incorporating a valid description of dispersion in saturated shales.

Acknowledgement

The authors acknowledge financial support from The Research Council of Norway, AkerBP, DONG Energy, ENGIE, Maersk and Total through the PETROMAKS 2 KPN-project: Shale Rock Physics: Improved seismic monitoring for increased recovery at SINTEF Norway (Grant no. 234074/E30). We also thank BP Houston for permission to include data obtained with one of their shale cores. The Research Council of Norway is also acknowledged for partial support through the "ROSE" project "Geophysical methods for subsurface imaging and monitoring", grant number 228400, at NTNU.